

*Original Research*

# Antimony Ore Tailings: Heavy Metals, Chemical Speciation, and Leaching Characteristics

Yingying Zhou<sup>1,2</sup>, Bozhi Ren<sup>1,2\*</sup>, Andrew S Hursthouse<sup>1,3</sup>, Saijun Zhou<sup>2</sup>

<sup>1</sup>Hunan Provincial Key Laboratory of Shale Gas Resource Exploitation, Xiangtan, China

<sup>2</sup>School of Civil Engineering, Hunan University of Science and Technology, Xiangtan, China

<sup>3</sup>School of Science and Sport, University of the West of Scotland, Paisley, United Kingdom

*Received: 3 December 2017*

*Accepted: 2 February 2018*

## Abstract

Antimony ore tailings slag was used to analyze heavy metals, chemical speciation, and leaching characteristics. The results show that the residual silicate phases account for 65.44% of Sb, 77.22% of As, 87.94% of Hg, 58.53% of Pb, 71.27% of Cd, and 96.34% of Zn. Although the exchangeable and carbonate phases account for 7.71% of Sb, 0.71% of As, 3.77% of Hg, 4.82% of Pb, 1.83% of Cd, and 1.73% of Zn, the water-or-acid-soluble phases contribute more to the chemical speciation of heavy metals. Concentrations of Sb, As, and Hg in the leachates increased with increasing solid-liquid ratio, decreasing particle size and increasing temperature. In simulated rainfall conditions, the total quantity increased in the order Sb > As > Hg and were 42.508 mg, 52.940 µg, and 0.876 µg, respectively, at 500 g antimony ore tailings. Under different rainfall intensity simulations, the maximum quantity in the leachates of Sb, As, and Hg were 93.894 mg, 255.451 µg, and 1.690 µg, respectively, and increased in the order of moderate > heavy > rainstorm. Finally, the cumulative leaching of Sb at pH 6.0 is 42.025 mg/L (higher than at 4.0 and 5.0), and the As and Hg at pH 4.0 are 107.097 µg/L and 0.989 µg/L, respectively.

**Keywords:** antimony ore tailings, heavy metals, speciation, leaching

## Introduction

Typically, tailings, as solid waste, are discharged into rivers or are contained in tailing dams. Antimony ore tailings contain Sb, As, Hg, and other heavy metals [1-4] that are highly toxic [5-7]. Previous reports have shown that the majority of heavy metals pollution appears to originate from mining and industry, because very high levels of pollution have been detected around tailings [8-11]. The pollution of heavy metals in the

aquatic environment results from rock weathering, soil runoff, and anthropogenic activities. The heavy metals in antimony ore tailings slowly precipitate into the soil and pollute surrounding areas, threatening the health and safety of humans and animals [12-15].

Presently, the leaching behavior of heavy metals in slag is based on static and dynamic leaching laboratory tests. Biver and Shotyk [16-17] derived an equation to describe the release of Sb from studying stibliconite, senarmontite, and valentinite ores and derived an empirical equation of the release of Sb from stiblite (Sb<sub>2</sub>S<sub>3</sub>). Zhang et al. [18] demonstrated that ultrasonic treatment can significantly shorten the time Sb and Pb

\*e-mail: yingzhouq@163.com

reach equilibrium in leaching tests of tailing slags. Hu et al. [10] found no significant correlation between Sb, As, Pb, and Cr leaching and heavy metals content in ores based on static leaching tests with acid solutions (pH = 2). Ren et al. [19-20] studied the leaching of Sb by static and dynamic leaching tests of antimony smelting slag. As we know, in the natural environment the oxidative dissolution of abundant sulfide ore leads to the net release of protons, a phenomenon known as acid mine or acid rock drainage [21-24]. Therefore, it is great significant to study the heavy metals, chemical speciation, and leaching characteristics in antimony ore tailings.

As the world's largest antimony (Sb) producer, China produces on average 80% of global Sb annually. Xikuangshan in Hunan, the world's largest Sb mine, is reported to produce 25% of the world's total [25]. The Xikuangshan mine has been mining for almost 120 years. Its longtime and large-scale mining has produced a large tailings storehouse. Harmful elements like Sb, As, and Hg have been released with surface runoff and precipitation infiltration, threatening the environment and human beings. Some reports shown that high Sb concentration in water (up to 29.4 mg/L), sediments (up to 1,163 mg/kg), and soils (up to 5,045 mg/kg) were found near Xikuangshan mining and smelting areas in China [26-28]. At present, the research mainly focuses on the removal of heavy metals in wastewater and the impact on the surrounding environment [29-32], but few have paid attention to the characteristics of metal dissolution in tailings and accumulated empirical equations. In this study, antimony ore tailings were studied with respect to heavy metals content, chemical speciation, and leaching characteristics to understand the leaching of heavy metals and derive accumulated empirical equations. It aims to provide theoretical support for the discharge and stockpiling of Sb, As, and Hg, etc., metal(loid) pollution control, and environmental monitoring. Other nonferrous mining areas can learn from research methods and conclusions

## Materials and Methods

### Materials

The antimony ore tailings were from the Lengshuijiang Xikuangshan Mine in China. The samples were air-dried and mixed, pulverized, and screened using nylon sieves with openings (20, 40, 60, and 100 mesh).

### Equipment and Methods

#### *Speciation of Heavy Metals in Tailings*

Metals in solid waste are associated with exchangeable (dissolved) cations, carbonates, Fe-Mn oxides, organic matter-sulfides complexes, and mineral residue [33]. In this study we used hydride generation atomic fluorescence spectrometry (HG-AFS) to determine the heavy

metals in the tailings, and modified Tessier sequential extraction [34] was used to examine the speciation of heavy metals.

#### *Heavy Metals in Tailings*

Antimony ore tailings with particle size less than 100 mesh were weighed with precision of 0.1 g into polytetrafluoroethylene digestion tanks, with 5 mL HNO<sub>3</sub> and 0.5 mL HF, and placed in an oven at 170°C for 12 h. Next, one mL 30% H<sub>2</sub>O<sub>2</sub> was added, and the solution was left to cool for 30 min; finally, 10 mL 5% HNO<sub>3</sub> was added. The sample was then filtered in a tubular filter with a 0.2- $\mu$ m polyethylene film, and ultrapure water (18.0 M $\Omega$ .cm) was added up to 50 mL. The heavy metals were measured by HG-AFS (AFS - 9700, Beijing Haiguang).

#### *Static Leaching Experiments*

The reactors were 1,000-mL glass bottles. The supernatant was extracted every 24 h, filtered in a tubular filter with 0.2- $\mu$ m polyethylene film, and the filtrate was analyzed by HG-AFS. All the experiments were performed in duplicate and with procedural blanks. The test periods were 12 days.

Antimony ore tailings with particle size more than 100 mesh were weighed (100, 50, and 25 g) and placed in the reactors with 500-mL ultrapure water. The pH of the solutions was adjusted to 7.0. The supernatant was extracted every 24 h. The concentration of heavy metals and the pH in the supernatant was measured at different soaking times and solid-liquid ratios (1:5, 1:10, 1:20).

Samples (50 g) with particle size of >100 mesh, 40-100 mesh, and 20-40 mesh were placed in the reactors with 500-mL ultrapure water (solid-liquid ratio of 1:10). The supernatant was extracted every 24 h. The concentration of heavy metals in the supernatant was measured at different soaking times.

Samples (50 g) with particle size >100 mesh were placed in the reactors with 500 mL ultrapure water (solid-liquid ratio of 1:10). The reactors were placed in a thermostatic chamber at 15°C, 25°C, and 35°C at different soaking times.

#### *Dynamic Leaching Experiments*

The leaching columns were polymethyl methacrylate tubes (Fig. 1) loaded from the bottom to the top in the following sequence: filter, fabrics, 50-mm-thick quartz sand (1-5 mm particle size), and 500 g of ore sample. The leaching columns were gently vibrated to compact the samples. Then a filter layer was placed on top of the sample to evenly distribute the water during leaching. Finally, 500 mL of ultrapure water was added and the entire setup was left to dry for 24 h. The leaching solution was H<sub>2</sub>SO<sub>4</sub>:HNO<sub>3</sub> (3:1 v/v) mixed with NaOH at different pH values to model various acid rain conditions. The test period was 12 days.

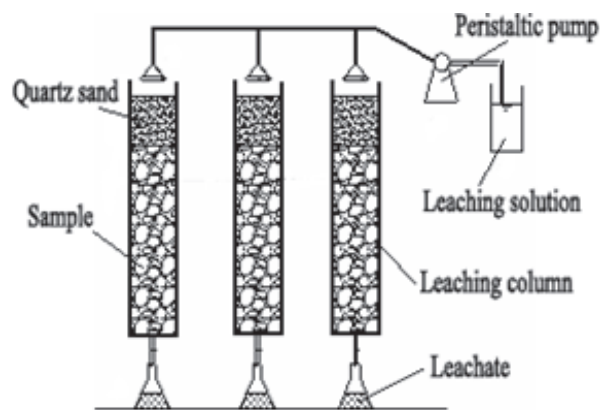


Fig. 1. Experimental setup in the dynamic leaching experiments.

The average rainfalls from January to December were 95, 98, 162, 224, 315, 324, 197, 185, 104, 110, 99, and 72 ml/month. One day's rainfall simulates a month's rainfall, the leaching solution (pH 5.0) was added by using a peristaltic pump and flow rate of 30 mL/h. Finally, the leaching solution was collected and the heavy metals concentration was measured.

To simulate the effect of rainfall intensity on leaching, leaching solution (pH 5.0) was daily added using a peristaltic pump up to 287 mL. The leaching rate was 60, 120, and 180 mL/h to simulate rainstorm, heavy rain, and moderate rain, respectively. Finally, the leaching solution was collected and the heavy metals concentration was measured.

To simulate the effect of variable pH on leaching and the release of heavy metals, 165 mL (monthly mean rainfall) of leaching solution with pH values of 4.0, 5.0, and 6.0 at flow rate of 60 mL/h was added daily using a peristaltic pump. Finally, the leaching solution was collected and the heavy metals and pH were measured.

*Analysis*

The concentration of Sb was determined by flame atomic absorption spectrophotometry (AA-7002A, Beijing Sanxiong) when the concentration of Sb was greater than 0.5 mg/L. The concentrations of As, Hg, and Sb (the concentration of Sb was below 0.5 mg/L) were determined by HG-AFS (AFS-9700, Beijing Haiguang). The pH of the leaching solution was measured using a pH meter (PB-10, Germany). The structure, morphology, and composition of antimony ore tailings before and

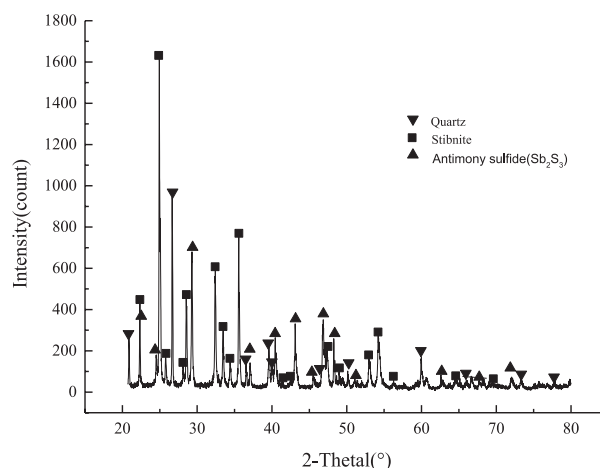


Fig. 2. XRD patterns of ore tailings.

after the static and dynamic leaching experiments were observed by transmission electron microscopy (JEOL JEM-2800, Japan), x-ray diffraction (XRD, SMART APEX, Germany), and the conditions of XRD were Cu K<sub>α</sub> radiation, 40 kV, and 40 mA, 2 theta range 10-80° with a scan rate step of 0.05°/s, and energy-dispersive spectroscopy (GENESIS, USA).

**Results and Discussion**

**Phase Composition**

The XRD patterns of the tailings were shown in Fig. 2. The results show that the antimony ore tailings mainly include stibnite, antimony sulfide, and quartz. Other minerals may not be detected because of the low content.

**Heavy Metals in Tailings**

The situation of heavy metal in tailings samples are given in Table 1. Five heavy metals exceed the background values.

**Chemical Speciation**

The elements of Sb, As, Hg, Pb, Cd, and Zn in antimony ore tailings were analyzed by the modified Tessier sequential extraction and the results are shown in Table 2. The bioavailability of heavy metal elements is closely related to chemical speciation. High

Table 1. Heavy metal content in antimony tail slag (mg/kg).

Heavy metal	Sb	As	Hg	Pb	Cd	Zn
Contents	2,570.43	984.25	3.11	19.18	2.08	577.35
Background values	2.98	14	0.09	27	0.079	95
Excess multiples	863	70	35	--	26	6

Table 2. Results of chemical speciation analysis for Sb, As, Hg, Pb, Cd, and Zn (mg/kg).

Antimony ore tailings												
	Sb		As		Hg		Pb		Cd		Zn	
	Concentration	%										
Exchange cations	47.30	1.84	4.33	0.44	0.04	1.29	0.092	0.48	0.026	1.27	6.75	1.17
Carbonates	150.88	5.87	2.66	0.27	0.077	2.48	0.832	4.34	0.012	0.56	3.23	0.56
Fe-Mn oxides	111.810	4.35	63.09	6.41	0.033	1.07	2.098	10.94	0.119	5.74	5.02	0.87
Organic matter-sulfide complexes	578.35	22.5	154.13	15.66	0.225	7.22	4.931	25.71	0.44	21.16	6.136	1.06
Residue	1,682.09	65.44	760.04	77.22	2.735	87.94	11.226	58.53	1.483	71.27	556.22	96.34
Total	2,570.43	100	984.25	100	3.11	100	19.18	100	2.08	100	577.35	100

bioavailability included water-soluble and exchangeable phases; moderate bioavailability included carbonates, Fe-Mn oxides, and organic matter-sulfide complexes. Low bioavailability included residual phases, typically

silicates. In the tailings, the exchangeable and carbonate phases mostly contributed to the leachates [33].

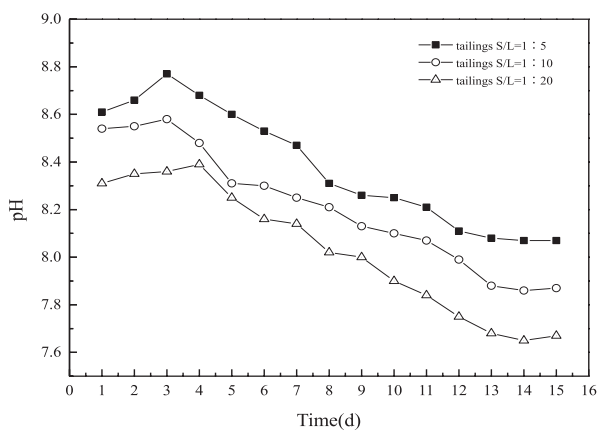


Fig. 3. Slag pH vs. time at different solid-liquid ratios.

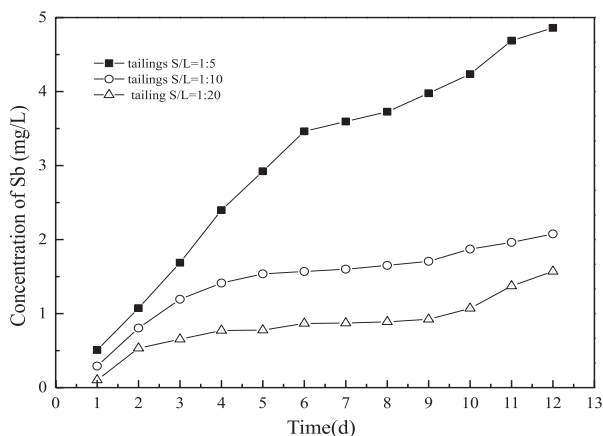


Fig. 4. Sb concentrations in leachate vs. time at different solid-liquid ratios.

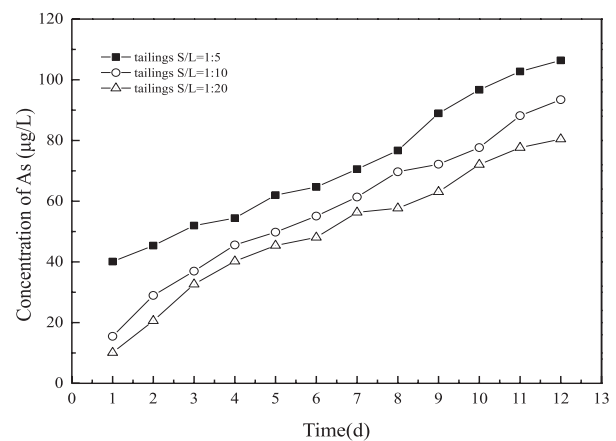


Fig. 5. As concentrations in leachate vs. time at different solid-liquid ratios.

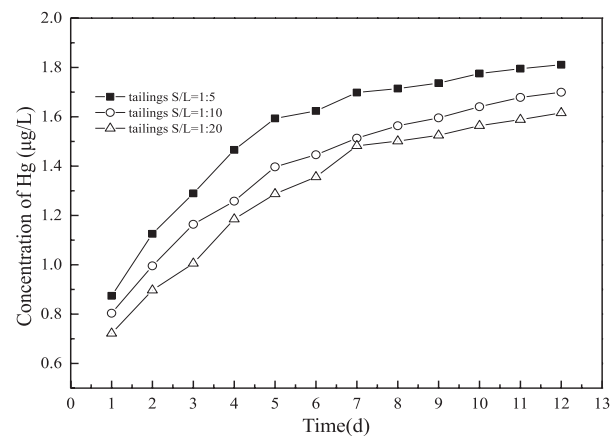


Fig. 6. Hg concentrations in leachate vs. time at different solid-liquid ratios.

In the tailings, the residual silicate phases account for 65.44% of Sb, 77.22% of As, 87.94% of Hg, 58.53% of Pb, 71.27% of Cd, and 96.34% of Zn. The exchangeable and carbonate phases account for 7.71% of Sb, 0.71%

of As, 3.77% of Hg, 4.82% of Pb, 1.83% of Cd, and 1.73% of Zn. Although the proportion of exchangeable and carbonate phases in tailings was small, the water-acid-soluble phases contributed more to the chemical speciation of heavy metals and produced a lot of pollution. Various forms would be transformed into each other [35].

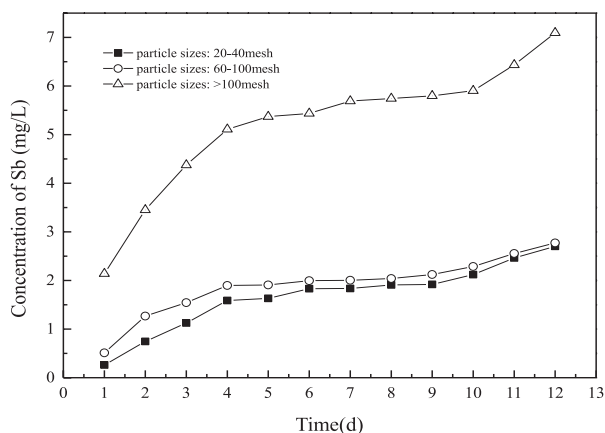


Fig. 7. Sb concentrations in the leachate vs. time at different particle sizes.

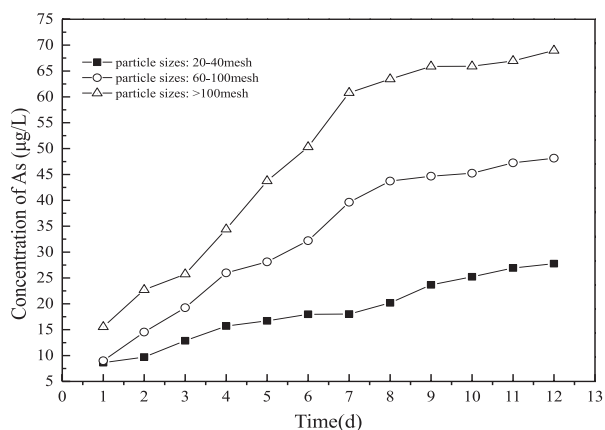


Fig. 8. As concentrations in the leachate vs. time at different particle sizes.

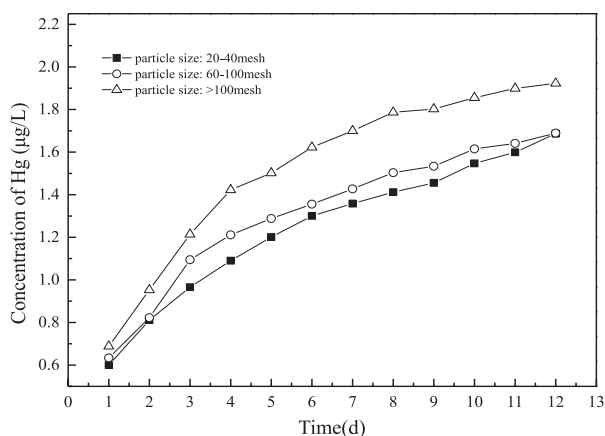


Fig. 9. Hg concentrations in the leachate vs. time at different particle sizes.

## Release of Heavy Metals

The release characteristics of heavy metals in antimony ore tailings under different solid-liquid ratio, particle size, leaching pH value, rainfall intensity and other condition were studied by dynamic and static leaching test. Accumulated empirical equations of heavy metals were established with different pH and different rainfall intensities.

### Solid-Liquid Ratio and Dissolution of Sb, As, and Hg

The pH and concentrations of Sb, As, and Hg with time at different solid-liquid ratios are shown in Figs 3-6. The soaking solution pH increased with increasing solid-liquid ratios and reached maximum (pH>8.0) after 3 to 4 days. This may be related to the alkaline composition of tailings, e.g., quartz. Subsequently, pH gradually decreased with time and then stabilized owing to the formation of  $H_2SO_4$  by the degradation of  $Sb_2S_3$  [36].

Figs 4-6 show changes in the concentrations of Sb, As, and Hg with time. Concentrations of Sb, As, and Hg in the soaking solution were low with small solid-liquid ratios. With increasing solid-liquid ratios, the concentrations of Sb, As, and Hg in the soaking solution increased. Dilution was important in the dissolution of heavy metals with decreasing solid-liquid ratios and was responsible for the low concentration of heavy metals. Small solid-liquid ratios may favor the dissolution of insoluble minerals.

The concentration of Hg in the soaking solution increased with time and stabilized, and the concentrations of Sb and As increased slowly after 10-12 days. Presumably, the process of dissolution started at the surface, then to the interior of the slag and became diffusion-dependent. The main influence factor that affects the analysis of static immersion is hydrolysis oxidation reaction on the waste surface [37].

### Particle Size and the Dissolution of Sb, As, and Hg

The dissolution of Sb, As, and Hg with different particle sizes is shown in Figs 7-9. Heavy metals dissolve faster and their concentrations in the solution were higher with decreasing particle size. The smaller the particle size the greater the surface area, and the greater the surface area in contact with liquid, the faster and more pronounced the dissolution of heavy metals in the tailings. In addition, the smaller the particle size,

the easier the dissociation of antimony mineral monomers, and thus the greater release of heavy metals into the liquid. With the decrease of particle size, the specific surface area and the reaction contact area increases, which makes the reaction rate accelerate so that the release amount increased [19].

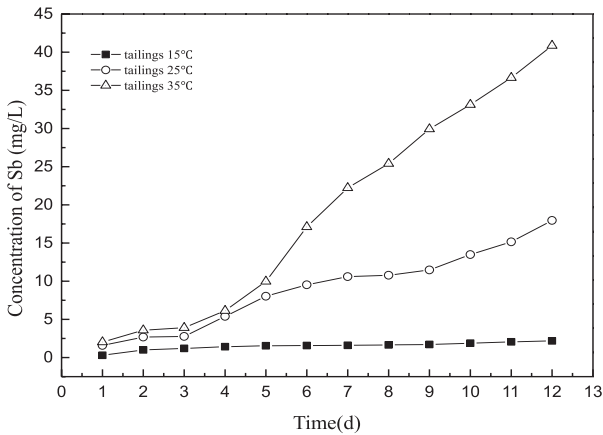


Fig. 10. Sb dissolution vs. time at different temperatures.

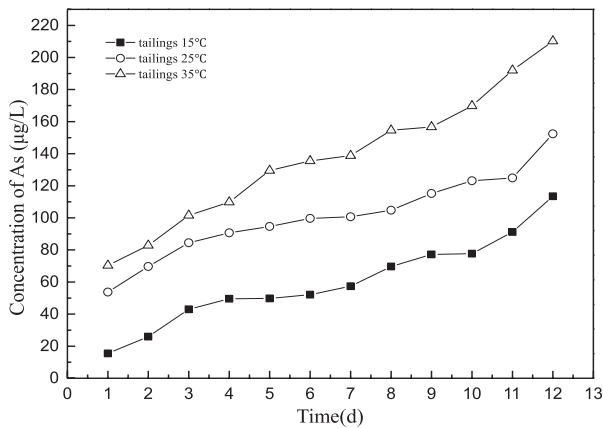


Fig. 11. As dissolution vs. time at different temperatures.

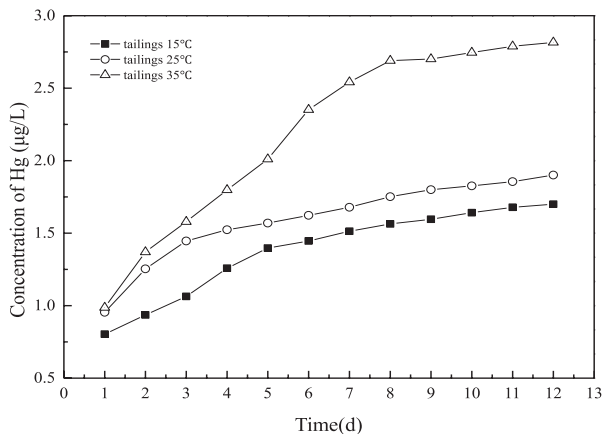


Fig. 12. Hg dissolution vs. time at different temperatures.

Temperature and the Dissolution of Sb, As, and Hg

The concentrations of Sb, As, and Hg in the soaking solution at different temperatures is shown in Figs 10-12. The process of dissolution was endothermic; therefore, the dissolution of heavy metals was favored by high temperatures. The influence of Sb and Hg was stronger than As At 35°C, whereas the influence was similar for Sb, As, and Hg at 15°C. According to the principle of chemical reaction equilibrium, when the temperature rises, the reaction moves in an endothermic direction.

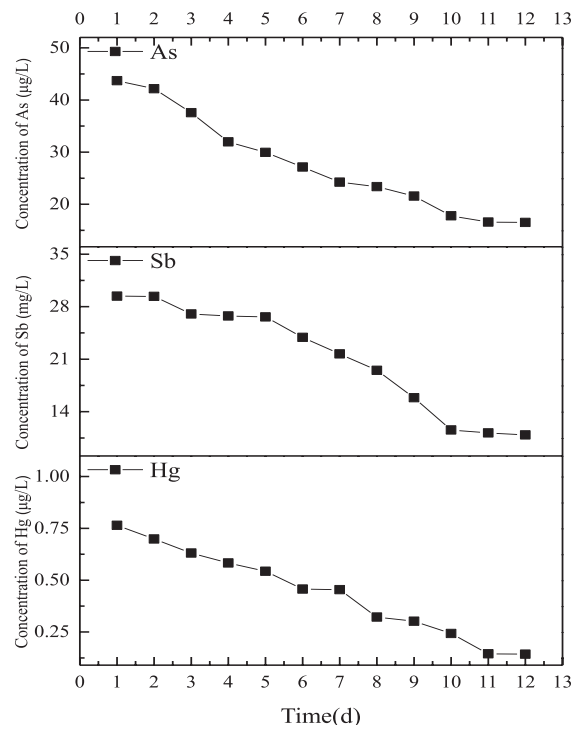


Fig. 13. Concentrations of Sb, As, and Hg vs. time in the dynamic leaching experiments.

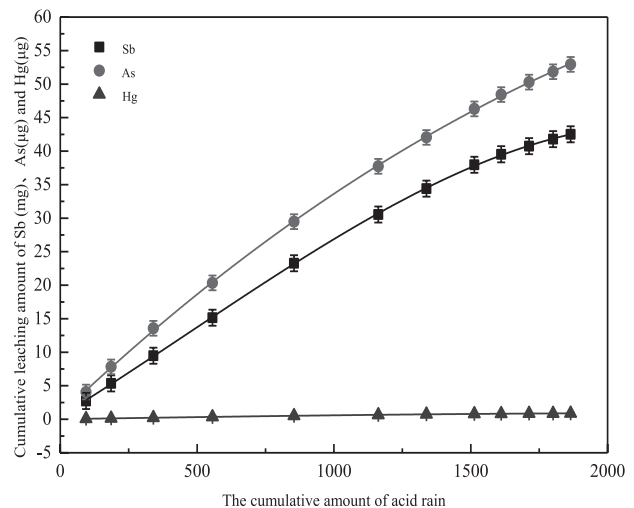


Fig. 14. Cumulative leaching of Sb, As, and Hg.

Therefore, heavy metals in antimony mining waste stone are more easily precipitated with higher temperature.

*Leaching Characteristic of Sb, As, and Hg*

The concentrations of Sb, As, and Hg vs. time in the acid rain simulations are shown in Fig. 13. The dissolution of Sb, As, and Hg is high initially and then decreases gradually. The release descending at the start of the leaching time may be because the surface pores of slag are eroded, leading to surface collapse and reduction of the contact area among slag, water, and air. The process of dissolution started at the surface of the particles. The diffusion of heavy metals from the residue to the solution was divided into disassociation from the solid-liquid interface and then dispersion from the solid-liquid interface to the solution. The first stage was fast, whereas the second was slow. The prolonged dissolution of heavy metals into the solution depends on diffusion, and the cumulative release is better described by cubic polynomials (Fig. 14).

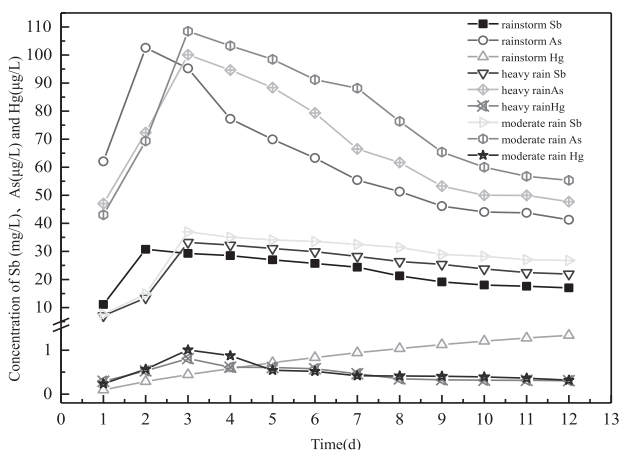


Fig. 15. Leaching behavior of heavy metals in the tailings under different rainfall intensities.

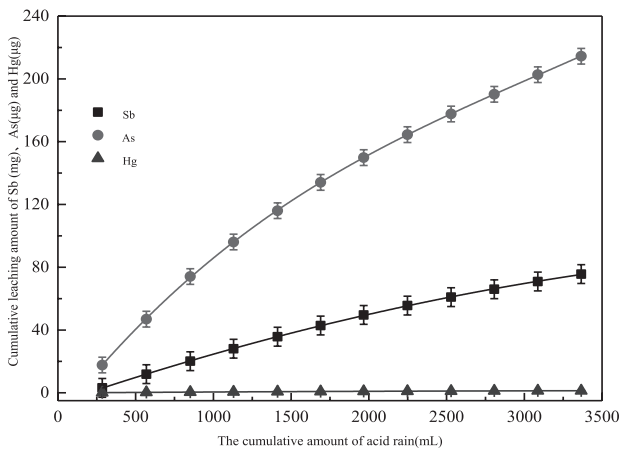


Fig. 16. Cumulative leaching data for Sb, As, and Hg during rainstorms.

The total quantity in the leachates increased in the order Sb > As > Hg and were 42.508 mg, 52.940 µg, and 0.876 µg, respectively, at 500 g antimony ore tailings. In the simulation of one year of acid rain, the concentration of Sb were 10.909 mg/L, As was 16.528 µg/L, and Hg was 0.133 µg/L.

Fitting equation of Sb:  $Y = 0.43978 + 0.0252X + 4.28974E^{-6}X^2 - 3.06015E^{-9}X^3$  ( $R^2 = 0.9999$ )

Fitting equation of As:  $Y = 0.69092 + 0.03894X - 6.19734E^{-6}X^2 + 2.04278E^{-10}X^3$  ( $R^2 = 0.9998$ )

Fitting equation of Hg:  $Y = 0.01491 + 6.30686E^{-4}X - 1.37286E^{-8}X^2 - 4.08827E^{-11}X^3$  ( $R^2 = 0.9998$ ).

*Leaching Characteristic of Sb, As, and Hg at Different Rainfall Intensities*

The average annual rainfall at Xikuangshan Mine was 1,440 mm, and the monthly rainfall was uneven. In this study, to simulate the rainfall, the average monthly rainfall for Lengshuijiang in 1995-2013 between April and June was considered along with the rainwater runoff

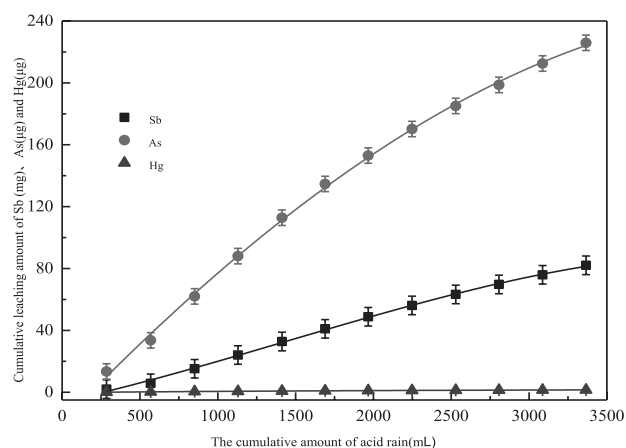


Fig. 17. Cumulative leaching data for Sb, As, and Hg during heavy rain.

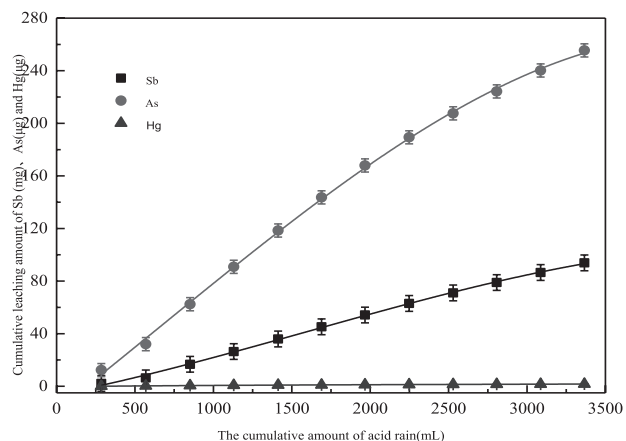


Fig. 18. Cumulative leaching data for Sb, As, and Hg during moderate rain.

loss. Consequently, the volume of water was 287 mL every day, the pH of water was 5.0.

The leaching behavior of Sb, As, and Hg at different rainfall intensities with time is shown in Fig. 15. The concentrations of Sb and As in the leachates peaked after 2 rainstorm days, whereas the Hg concentration was lowered. The concentrations of Sb, As, and Hg in the leachates peaked after 3 days of heavy or moderate rain, reaching the maximum and then gradually stabilizing. Comparing rainstorms with heavy and moderate rain, the hydraulic shear forces on the surface of the particles was high and thus scouring forces were also higher than

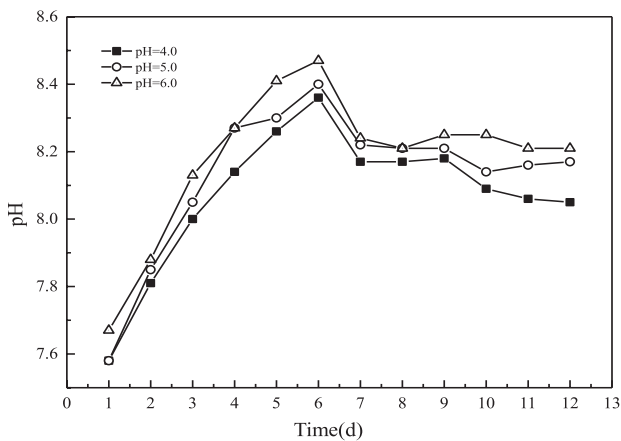


Fig. 19. pH value of leaching solutions vs. time for different initial pH solutions.

in other conditions [38]. Therefore, the concentration of heavy metals in the runoff peaked early and quickly reached maximum. However, the larger intensity signs and the shorter duration with the same level of rainfall means the leaching time and oxidation precipitation will be reduced.

The leaching behavior of heavy metals depends on the rainfall intensity, and for rainstorms were 75.650 mg, 214.440 µg, and 1.339 µg, for Sb, As, and Hg, respectively. For heavy rain, the Sb, As, and Hg quantities in the leachates were 82.073 mg, 225.902 µg, and 1.535 µg, respectively. Finally, for moderate rain, the quantities of Sb, As, and Hg in the leachates were 93.894 mg, 255.451 µg, and 1.690 µg, respectively. The leaching of Sb, As, and Hg increased in the following order: moderate rain > heavy rain > rainstorm.

The leaching of heavy metals was complex and involves vertical motion, horizontal diffusion, and other physical and chemical processes. Finally, cubic polynomials better described the experimental results for the cumulative release and rainfall (Figs 16-18).

Rainstorm:

Fitting equation of Sb:  $Y = -6.4176 + 0.03384X - 2.79454E^{-6}X^2 - 1.12441E^{-11}X^3$  ( $R^2 = 0.9998$ )

Fitting equation of As:  $Y = -16.09143 + 0.12581X - 2.67666E^{-5}X^2 + 2.8964E^{-9}X^3$ , ( $R^2 = 0.9999$ )

Fitting equation of Hg:  $Y = -0.09502 + 7.22529E^{-4}X - 1.15296E^{-7}X^2 + 8.14254E^{-12}X^3$  ( $R^2 = 0.9998$ )

Heavy rain:

Fitting equation of Sb:  $Y = -6.22899 + 0.02235X + 5.07232E^{-6}X^2 - 1.18142E^{-9}X^3$  ( $R^2 = 0.9984$ )

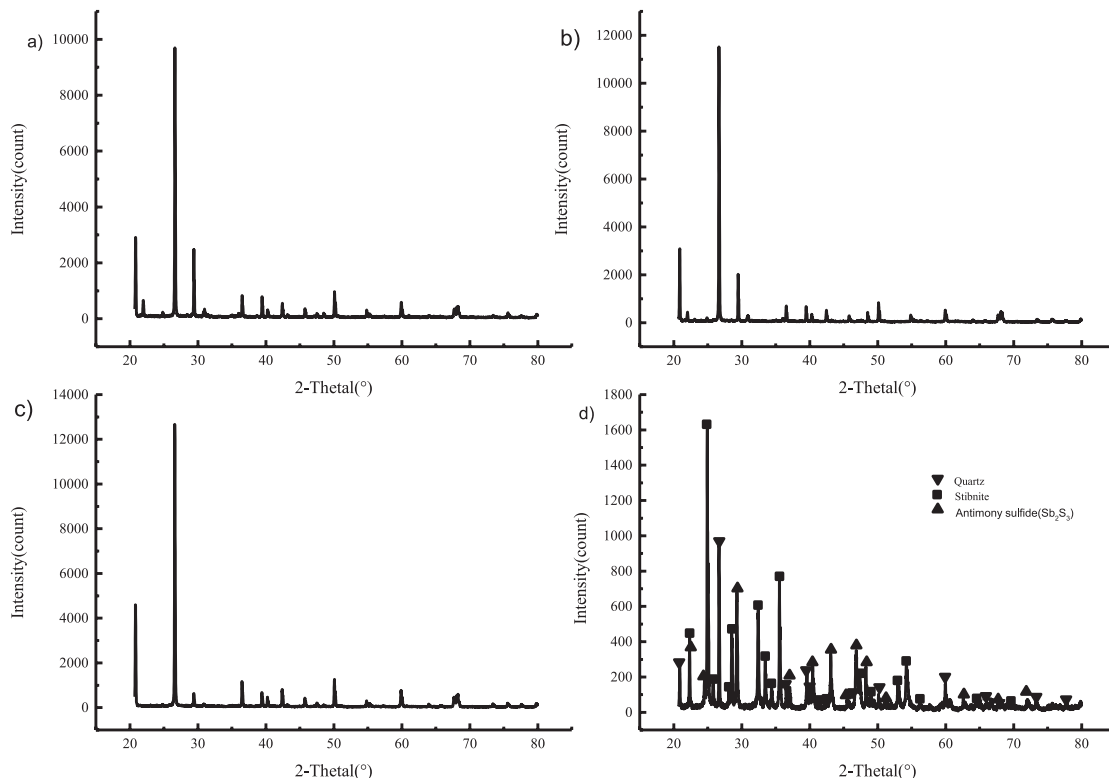


Fig. 20. XRD patterns of leaching residues at a) pH 4.0, b) pH 5.0, c) pH 6.0, and d) slag.

Table 3. Slag composition before and after leaching (% mass fraction).

	O	Si	Al	Ca	S	Pb	Cd	Sb	As	Hg	Cu	Mn	K	Fe	Cr
Before leaching	43.38	47.07	1.63	1.47	0.86	1.33	0.18	1	0.02	0.48	0.53	1.07	0.37	1.09	0.05
After leaching	52.55	40.34	1.34	0.89	0.09	1.22	0.06	0.82	0.48	0.45	0.32	0.67	0.02	0.63	0.03

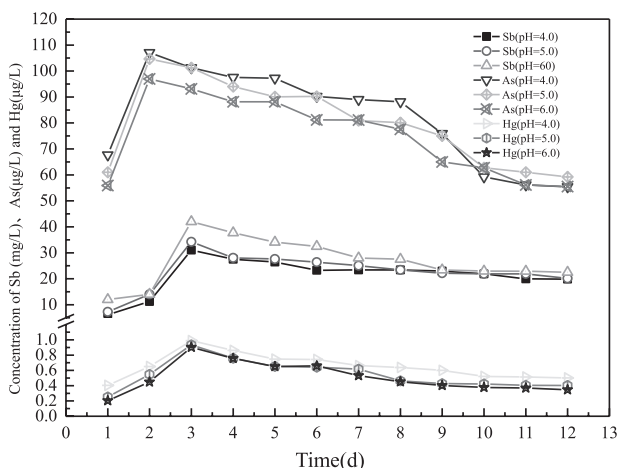


Fig. 21. Concentrations of Sb, As, and Hg in the leachate vs. time at different initial solution pH.

Fitting equation of As:  $Y = -19.03855 + 0.10466X - 8.20287E^{-6}X^2 - 4.23241E^{-10}X^3$  ( $R^2 = 0.9987$ )

Fitting equation of Hg:  $Y = -0.1726 + 8.40574E^{-4}X - 1.15315E^{-7}X^2 + 4.48919E^{-12}X^3$  ( $R^2 = 0.9981$ )

Moderate rain:

Fitting equation of Sb:  $Y = -6.49908 + 0.02345X + 6.22811E^{-6}X^2 - 1.30453E^{-9}X^3$  ( $R^2 = 0.9987$ )

Fitting equation of As:  $Y = -18.13551 + 0.09377X + 5.3482E^{-6}X^2 - 2.74515E^{-9}X^3$  ( $R^2 = 0.9980$ )

Fitting equation of Hg:  $Y = -0.26782 + 0.00112X - 2.47942E^{-7}X^2 + 2.64602E^{-11}X^3$  ( $R^2 = 0.9967$ )

#### Leaching Characteristics of Sb, As, and Hg at Different pH

The evolution of pH in the leaching solutions with time is shown in Fig. 19. The pH of the leachates increased in the first six days, then decreased, and finally stabilized. The high pH values are due to the strong neutralizing ability of alkaline minerals, such as quartz, in the tailings [39]. The leachate pH values influenced the metals precipitation to an extent [36, 40].

In Fig. 20, the diffraction peaks of quartz and calcite decreased after leaching and this is consistent with leaching affecting stibnite, antimony sulfide, and quartz. From the energy spectrum in Table 3, it was inferred that  $Al^{3+}$  in the tailings reacts with  $OH^-$  and sulfide minerals ( $FeAsS$ ) oxidizing to produce  $H_2SO_4$  and  $Fe_2(SO_4)_3$  [41], decreasing the pH of the leaching solution [42].

The concentrations of Sb, As, and Hg in the leachates with time at different initial pH are shown in Fig. 21.

The Sb, As, and Hg concentrations rapidly reached maximum within one to 3 days. This may be due to the destruction of the particle surface structure and the oxidation of phases, such as  $Sb_2S_3$  to  $SbO_3^-$ , to form complexes that enter the leachate [43].  $Al^{3+}$  and  $Fe^{3+}$  reacted with the weak alkaline solutions to produce colloids that cover the surface of the slag particles, preventing further oxidation. Compared with As and Hg, the concentration of Sb changes inversely, which was related to Sb having both sexes.

From Fig. 21, the change trend of concentrations about As and Hg were same, and concentrations of As under initial pH = 4.0, pH = 5.0, and pH = 6.0 leaching solution reached the maximums after 2 days, which were  $107.097 \mu\text{g}\cdot\text{L}^{-1}$ ,  $104.608 \mu\text{g}\cdot\text{L}^{-1}$ , and  $96.973 \mu\text{g}\cdot\text{L}^{-1}$ , respectively. The concentrations of Hg under initial pH = 4.0, pH = 5.0, and pH = 6.0 leaching solution reached maximum after 3 days:  $0.989 \mu\text{g}/\text{L}$ ,  $0.934 \mu\text{g}/\text{L}$ , and  $0.902 \mu\text{g}/\text{L}$ , respectively. The exchangeable phases were oxidized and fully released of heavy metals to the solutions, which made the curve appear on a downward trend and determined the final concentration of heavy metals [44].

## Conclusions

The contents of Sb, As, Hg, Cd, and Zn in antimony ore tailings exceed the background values in the order of  $Sb > Cd > Hg > Zn > As$ . The chemical speciation of heavy metals in the tailings was mainly due to the residual phases, whereas the content of exchangeable cations and carbonate minerals was low, but those were mainly the chemical speciation of pollution.

The leaching behaviors of Sb, As, and Hg were examined with different solid-liquid ratios, particle sizes, temperatures, pH, and rainfall intensities. In the leachates, the concentrations of Sb, As, and Hg increased with increasing solid-liquid ratio, decreasing particle size, and increasing temperature. Leaching as a function of rain increased in the order of moderate rain > heavy rain > rainstorm. The cumulative leaching of Sb at pH 6.0 was higher than that at pH 4.0 and 5.0, and the cumulative leaching of As and Hg increased in the order of pH 4.0 > pH 5.0 > pH 6.0.

## Acknowledgements

This work was supported by the National Natural Science Foundation of China (No. 41472328).

### Conflict of Interest

The authors declare no conflict of interest.

### References

- ELSHARJAWY A.A., AMIN A.S.. Use of cloud-point preconcentration for spectrophotometric determination of trace amounts of antimony in biological and environmental samples. *Analytical Biochemistry*. **492**, 1, **2016**.
- FORT M., GRIMALT J.O., QUEROL X., CASAS M., SUNYER J. Evaluation of atmospheric inputs as possible sources of antimony in pregnant women from urban areas. *Science of the Total Environment*. **544**, 391, **2016**.
- SHARIFI R., MOORE F., KESHAVARZI B. Mobility and chemical fate of arsenic and antimony in water and sediments of Sarouq River catchment, Takab geothermal field, northwest Iran[J]. *Journal of Environmental Management*. **170** (02), 136, **2016**.
- SUN W., XIAO E., DONG Y., TANG S., KRUMINS V., NING Z., SUN M., ZHAO Y., WU S., XIAO T. Profiling microbial community in a watershed heavily contaminated by an active antimony (Sb) mine in Southwest China. *Science of the Total Environment*. **550**, 297, **2016**.
- WU F., FU Z., LIU B., MO C., CHEN B., CORNS W., LIAO H. Health risk associated with dietary co-exposure to high levels of antimony and arsenic in the world's largest antimony mine area. *Science of the Total Environment*. **409** (18), 3344, **2011**.
- PENG B., LIU Z., CHAI L., LIU H., YANG S., YANG B., XIANG K., LIU C. Effect of copper ions on the mercury re-emission in a simulated wet scrubber. *Fuel*, **2016**.
- LIU Z., WANG D., PENG B., CHAI L., LIU H., YANG S., YANG B., XIANG K., LIU C. Transport and transformation of mercury during wet flue gas cleaning process of nonferrous metal smelting. *Environmental Science & Pollution Research*. **24** (28), 22494, **2017**.
- GUO X., WANG K., HE M., LIU Z., YANG H., LI S. Antimony smelting process generating solid wastes and dust: characterization and leaching behaviors. **26** (7), 1549, **2014**.
- WILSON S.C., LOCKWOOD P.V., ASHLEY P.M., TIGHE M. The chemistry and behaviour of antimony in the soil environment with comparisons to arsenic: a critical review. *Environmental Pollution*. **158** (5), 1169, **2010**.
- HU X., HE M., KONG L. The leaching characteristics and changes in the leached layer of antimony-bearing ores from China. *Journal of Geochemical Exploration*. **176**, 76, **2016**.
- LI Y., LIU Z., LIU H., PENG B. Clean strengthening reduction of lead and zinc from smelting waste slag by iron oxide. *Journal of Cleaner Production*. **143**, 311, **2016**.
- BECH J., CORRALES I., TUME P., BARCELÓ J., DURAN P., ROCA N., POSCHENRIEDER C. Accumulation of antimony and other potentially toxic elements in plants around a former antimony mine located in the Ribes Valley (Eastern Pyrenees). *Journal of Geochemical Exploration*. **113** (1), 100, **2012**.
- BIVER M., SHOTYK W. Experimental study of the kinetics of ligand-promoted dissolution of stibnite (Sb<sub>2</sub>S<sub>3</sub>). *Chemical Geology*. **294-295** (4), 165, **2012**.
- SHTANGEEVA I., BALI R., HARRIS A. Bioavailability and toxicity of antimony [J]. *Journal of Geochemical Exploration*. **110** (1), 40, **2011**.
- SHTANGEEVA I., NIEMELÄ M., PERÄMÄKI P. Effects of soil amendments on antimony uptake by wheat[J]. *Journal of Soils & Sediments*. **14** (4), 679, **2014**.
- IBIVER M., SHOTYK W. Stibiconite (Sb<sub>3</sub>O<sub>6</sub>OH), senarmontite (Sb<sub>2</sub>O<sub>3</sub>) and valentinite (Sb<sub>2</sub>O<sub>3</sub>): Dissolution rates at pH 2–11 and isoelectric points. *Geochimica Et Cosmochimica Acta*. **109** (3), 268, **2013**.
- BIVER M., SHOTYK W. Stibnite (Sb<sub>2</sub>S<sub>3</sub>) oxidative dissolution kinetics from pH 1 to 11[J]. *Geochimica Et Cosmochimica Acta*. **79** (3), 127, **2012**.
- ZHANG R.L., ZHANG X.F., TANG S.Z., HUANG A.D. Ultrasound-assisted HCl–NaCl leaching of lead-rich and antimony-rich oxidizing slag. *Ultrasonics Sonochemistry*. **27**, 187, **2015**.
- REN B., ZHOU Y., HURSTHOUSE A.S. DENG R. Research on the Characteristics and Mechanism of the Cumulative Release of Antimony from an Antimony Smelting Slag Stacking Area under Rainfall Leaching. *Journal of Analytical Methods in Chemistry*. **2017** (4), 1, **2017**.
- REN B., ZHOU Y., MA H., DENG R., ZHANG P., HOU B. Sb release characteristics of the solid waste produced in antimony mining smelting process. *Journal of Material Cycles & Waste Management*. 1-8, **2016**.
- KWONG Y.T.J., WHITLEY G., ROACH P., EPPINGER R.G., FUGE R. Natural acid rock drainage associated with black shale in the Yukon Territory, Canada. *Applied Geochemistry*. **24** (2), 221, **2009**.
- VERPLANCK P.L., NORDSTROM D.K., BOVE D.J., PLUMLEE G.S., RUNKEL R.L., EPPINGER R.G., FUGE R. Naturally acidic surface and ground waters draining porphyry-related mineralized areas of the Southern Rocky Mountains, Colorado and New Mexico. *Applied Geochemistry*. **24** (2), 255, **2009**.
- ASTA M.P., AYORA C., ROMÁN-ROSS G., CAMA J., ACERO P., GAULT A.G., CHARNOCK J.M., BARDELLI F. Natural attenuation of arsenic in the Tinto Santa Rosa acid stream (Iberian Pyritic Belt, SW Spain): The role of iron precipitates. *Chemical Geology*. **271** (1-2), 1, **2010**.
- MONCUR M.C., JAMBOR J.L., PTACEK C.J., BLOWES D.W., THOMPSON A., VAUGHAN D.J. Mine drainage from the weathering of sulfide minerals and magnetite. *Applied Geochemistry*. **24** (12), 2362, **2009**.
- U.S. Geological Survey, Mineral Commodity Summaries 2013. Washington, **2013**.
- HE M., WANG X., WU F., FU Z. Antimony pollution in China. *The Science of the total environment*. **421-422** (3), 41, **2012**.
- M H. Distribution and phytoavailability of antimony at an antimony mining and smelting area, Hunan, China. *Environmental Geochemistry and Health*. **29** (3), 209, **2007**.
- LI J., WEI Y., ZHAO L., ZHANG J., SHANGGUAN Y., LI F., HOU H. Bioaccessibility of antimony and arsenic in highly polluted soils of the mine area and health risk assessment associated with oral ingestion exposure. *Ecotoxicology & Environmental Safety*. **110** (110), 308, **2014**.
- CIDU R., BIDDAU R., DORE E., VACCA A., MARINI L. Antimony in the soil–water–plant system at the Su Suergiu abandoned mine (Sardinia, Italy): Strategies to mitigate contamination. *Science of the Total Environment*. **497-498** (1), 319, **2014**.
- WANG X., HE M., XI J., LU X. Antimony distribution and mobility in rivers around the world's largest antimony mine

- of Xikuangshan, Hunan Province, China. *Microchemical Journal*. **97** (1), 4, **2011**.
31. TIGHE M., LOCKWOOD P., WILSON S. Adsorption of antimony(V) by floodplain soils, amorphous iron(III) hydroxide and humic acid. *J Environ Monit.* **7** (12), 1177, **2005**.
  32. MITSUNOBU S., MURAMATSU C., WATANABE K., SAKATA M. Behavior of antimony(V) during the transformation of ferrihydrite and its environmental implications. *Environmental Science & Technology*. **47** (17), 9660, **2013**.
  33. TESSIER A., CAMPBELL P.G.C., BISSON M. Particulate trace metal speciation in stream sediments and relationships with grain size: Implications for geochemical exploration[J]. *Journal of Geochemical Exploration*. **16** (2), 77, **1982**.
  34. LEE P.K., YU S. Lead isotopes combined with a sequential extraction procedure for source apportionment in the dry deposition of Asian dust and non-Asian dust. *Environmental Pollution*. **210**, 65, **2016**.
  35. ALABED S.R., HAGEMAN P.L., JEGADEESAN G., MADHAVAN N., ALLEN D. Comparative evaluation of short-term leach tests for heavy metal release from mineral processing waste. *Science of the Total Environment*. **364** (1–3), 14, **2006**.
  36. ZHOU S., LI N., REN B., ZHANG P. Release Law of Sb, As, and Hg in Antimony Smelting Slag Under Simulated Acid Rain. *Polish Journal of Environmental Studies*., **26** (2), 925, **2017**.
  37. ZHAO G.H., LUO X.Z., CHEN G., ZHAO Y.J. A long-term static immersion experiment on the leaching behavior of heavy metals from waste printed circuit boards. *Environmental Science Processes & Impacts*. **16** (8), 1967, **2014**.
  38. LIU H., LEI T.W., ZHAO J., YUAN C.P., FAN Y.T., QU L.Q. Effects of rainfall intensity and antecedent soil water content on soil infiltrability under rainfall conditions using the run off-on-out method[J]. *Journal of Hydrology*. **396** (1), 24, **2011**.
  39. QAJAR J., ARNS C.H. Characterization of reactive flow-induced evolution of carbonate rocks using digital core analysis- part 1: Assessment of pore-scale mineral dissolution and deposition. *Journal of Contaminant Hydrology*. **192**, 60, **2016**.
  40. POTYSZ A., KIERCZAK J., FUCHS Y., GRYBOS M., GUIBAUD G., LENS P.N.L., HULLEBUSCH E.D.V. Characterization and pH-dependent leaching behaviour of historical and modern copper slags. *Journal of Geochemical Exploration*. **160**, 1, **2016**.
  41. RIVERA-VASQUEZ B.F., DIXON D. Rapid atmospheric leaching of enargite in acidic ferric sulfate media. *Hydrometallurgy*. **152**, 149, **2015**.
  42. LI H., WANG Z., YANG Z., CHAI L., LIAO Y. Static and Dynamic Leaching of Chromium(VI) from Chromium-Containing Slag. *Environmental Engineering Science*. **29** (6), 426, **2012**.
  43. HU X., HE M., KONG L. Photopromoted oxidative dissolution of stibnite. *Applied Geochemistry*. **61**, 53, **2015**.
  44. KYZAS G.Z., MATIS K.A. Methods of arsenic wastes recycling: Focus on flotation. *Journal of Molecular Liquids*. **214**, 37, **2016**.

